

Supplemental materials and methods

Viral vectors

The coding sequence of P1A or the juxtaposed coding sequences of MAGE-A3 and NY-ESO-1 were inserted into the E1 locus of ChAdOx1 under a CMV immediate early promoter. A sequence coding for the 26 amino acid transmembrane domain of the MHC-II invariant chain with sequence fragment was linked to the N terminus of the transgene, described previously ¹. The MVA vectors encoding P1A, MAGE-A3 and NY-ESO-1 were constructed with or without the leader sequence of the human tissue plasminogen activator gene (tPA) with the F11 promoter driving transgene expression. Viral vectors were isolated and purified as described ². The purity and identity of the viral vectors were confirmed by PCR.

Tumor biopsy for gene expression analysis

Tumor masses were surgically excised and pieces ≤30 mg were immediately frozen in liquid nitrogen and stored at minus 80°C. Total cellular RNA was isolated using a RNeasy mini kit (Qiagen) with column-based RNase-free DNase I (Qiagen) digestion to remove genomic DNA, then used for gene expression analysis.

Reverse Transcription Quantitative PCR (RT-qPCR)

Total cellular RNA (0.5 µg) was used to synthesize first single-strand cDNA using the SuperScript III First-Strand Synthesis kit (Thermo Fisher). Reactions were performed according to the manufacturer's protocol. For quantification of cDNA by qPCR, the QuantiTect SYBR Green PCR kit (Qiagen) was used and reactions set up according to the manufacturer's instructions. Reactions were run on the StepOnePlus™ Real-Time PCR System (Applied Biosystems) at the following conditions – 95°C - 15 min, (94°C 15s + 60°C 30s + 72°C 30s) x 40 cycles. Gene expression at the mRNA level for each target gene assayed was quantified relative to an internal housekeeping gene control. The housekeeping genes

used were either *ActB* or *Hprt1*. To determine relative mRNA expression, the mean ΔCt (difference in cycle threshold number) was calculated for each target gene relative to *ActB* or *Hprt1*. ΔCt for a given target gene in each sample was therefore calculated according to the formula $\Delta Ct = Ct \text{ Target gene} - Ct \text{ Housekeeping gene}$. Relative mRNA expression data are shown as $2^{-\Delta Ct}$. The list of primers used is shown in table S1.

Table S1: qPCR primer sequences

Primer	Sequence (5'-3')
<i>Actb</i> for	CCTTCAACACCCCAGCCATGTA
<i>Actb</i> rev	GGATGGCGTGAGGGAGAGCAT
P1A for	AGCTGAGGAAATGGGTGCTG
P1A rev	CAGCATTTTCACACCTACACTCCA
<i>Hprt1</i> for	AGTGTGGATACAGGCCAGAC
<i>Hprt1</i> rev	CGTGATTCAAATCCCTGAAGT
<i>Cxc19</i> for	GCCATGAAGTCCGCTGTTCT
<i>Cxc19</i> rev	GGGTTCTCGAACTCCACACT
<i>Cxc10</i> for	GACGGTCCGCTGCAACTG
<i>Cxc10</i> rev	GCTTCCCTATGGCCCTCATT
<i>Ccl3</i> for	GCCAGGTGTCATTTTCCTGACTA
<i>Ccl3</i> rev	AGGCATTAGTTCCAGGTCA
<i>Ccl5</i> for	GCAAGTGCTCCAATCTTGCA
<i>Ccl5</i> rev	CTTCTCTGGGTTGGCACACA
<i>Ifng</i> for	CGGCACAGTCATTGAAAGCCTA
<i>Ifng</i> rev	GTTGCTGATGGCCTGATTGTC
<i>Xcl1</i> for	CTTCCTGGGAGTCTGCTGC
<i>Xcl1</i> Rev	CAGCCGCTGGGTTTGTAAAGT

Immunohistochemistry

Tumor tissue was fixed and embedded in paraffin. Tissue slices of 4 μm were rehydrated in a series of histo-clear and graded ethanol. The tissue sections were incubated at 95 °C with citrate buffer (pH 6) for antigen retrieval and blocked with 1 $\mu\text{g}/\text{mL}$ Rat IgG (Vector Lab) diluted into 2.5 % Normal Goat Serum (Vector Labs) before staining with rabbit polyclonal anti-CD8a (361003, Synaptic Systems), anti-CCL5 (clone 25H14L17, ThermoFisher) or anti-CXCL9 (clone 11H1L14, ThermoFisher). Then the slides were washed and were incubated with ImmPRESS HRP Reagent peroxidase Anti-Rabbit IgG (Vector Labs). The sections were developed using ImmPACT DAB Chromogen (Vector Labs) and stained with haematoxylin,

dehydrated in a graded series of ethanol and histo-clear and cover slipped. Immunostaining were imaged using NanoZoomer S210 Digital slide scanner.

Bulk RNA-sequencing data analysis

Fastq sequencing data files were trimmed of adapter sequences using Skewer³ and reads mapped to mouse genome GRCm38.ERCC using HISAT2 aligner⁴. A count matrix reporting the numbers of reads mapping to each gene was generated using the featureCounts program in the Subread UNIX package⁵ and gene expression was calculated as counts per million (CPM). Genes expressed at a level <1 CPM were excluded from further analysis. R package "edgeR" was used for data normalization and differential expression analysis⁶. Briefly, count data was normalized using the trimmed mean of M values (TMM) method and differential gene expression analysis between indicated samples determined using the glmQLFTest method. The Benjamini–Hochberg correction was applied to the list of differentially expressed genes to calculate corrected P-values (P_{adj}). Genes with a $P_{adj} < 0.05$ and an absolute $\log_2FC > 1$ were considered as differentially expressed. T-cell inflamed and IFN- γ -related mRNA gene expression signatures were defined and associated gene expression signature scores calculated as described by M. Ayers and colleagues⁷. Heatmaps showing \log_{CPM} gene expression values from TMM-normalized count data were generated using the pheatmap R package. Gene set variation analysis (GSVA) was performed using R package GSVA⁸. The gene ontology (GO) gene sets used were obtained from the Molecular Signatures Database⁹. Hierarchical clustering and heatmap visualization of the GSVA matrix was performed using R package pheatmap.

Single-cell RNA-sequencing (scRNA-seq) data analysis

scRNA-seq data were pre-processed using the 10x Genomics CellRanger at the Oxford Genomics Centre and further analyzed with the R package Seurat v3.1.4¹⁰. For spleen

samples, cells with less than 200 UMI or detected genes were filtered out. For tumor samples, cells with UMI less than 500 or detected genes less than 300 were filtered out. For both types of samples, cells with higher than 10 percent of transcripts mapping to mitochondrial gene were filtered out. In addition, 100 potential doublets were removed using R package *scDblFinder* v1.3.0¹¹. Finally, genes expressed in less than 5 cells were removed, leading to a total of 5,578 cells and 11,502 genes for analysis. SCTransform was used to normalize samples, regress out cell cycle differences and identify highly variable genes. Mitochondrial, cell cycle, ribosomal and pseudo genes were excluded from the variable genes and the top 2000 most variable genes were used for sample integration using Seurat's integration workflow. Prior to clustering, principal component analysis (PCA) was applied to the variable genes of the dataset to reduce dimensionality. The top 25 principal components were used for Seurat's K-nearest neighbor (KNN) graph-based clustering analysis and the resulting clusters were visualized using the Uniform Manifold Approximation and Projection (UMAP). Differential gene expression analysis was performed on the log-normalized data with Seurat v4.0.1 by the non-parametric Wilcoxon rank-sum test using the *FindMarkers* function followed by Bonferroni correction using all genes for adjusted p-value calculation. Top DEGs were visualized using *ComplexHeatmap* ver2.6.2. Gene signatures characterizing the four experimental groups were generated by using the DEGs, with an adjusted p-value < 0.01 and average log₂ fold change > 0.25, between combination therapy-treated and vaccine-treated single P1A₃₅₋₄₃-specific CD8⁺ T cells in the spleen and tumor, respectively. For single-cell gene signature scoring, log-normalized data was used as input with gene signature lists (Table S2), which include the four above-mentioned gene signatures, as well as stem-like and exhaustion signatures from other recent studies. Signature scores for all gene signatures were calculated using the

AddModuleScore function in Seurat followed by z-scale normalization for cross-signature comparison across cells. Clustered correlation matrix showing the Pearson correlation coefficients between various gene signatures from single P1A₃₅₋₄₃-specific CD8⁺ T cells was generated using R package Corrplot v0.84 and visualized after hierarchical clustering. Seurat's AverageExpression function was used to calculate the average expression of genes for each experimental group. Heatmaps were plotted using R package pheatmap v1.0.12.

References

1. Halbroth BR, Sebastian S, Poyntz HC, *et al.* Development of a Molecular Adjuvant to Enhance Antigen-Specific CD8(+) T Cell Responses. *Sci Rep* 2018;8:15020.
2. Dicks MD, Spencer AJ, Edwards NJ, *et al.* A novel chimpanzee adenovirus vector with low human seroprevalence: improved systems for vector derivation and comparative immunogenicity. *PLoS One* 2012;7:e40385.
3. Jiang H, Lei R, Ding SW, *et al.* Skewer: a fast and accurate adapter trimmer for next-generation sequencing paired-end reads. *BMC Bioinformatics* 2014;15:182.
4. Kim D, Langmead B, Salzberg SL. HISAT: a fast spliced aligner with low memory requirements. *Nat Methods* 2015;12:357-60.
5. Liao Y, Smyth GK, Shi W. featureCounts: an efficient general purpose program for assigning sequence reads to genomic features. *Bioinformatics* 2014;30:923-30.
6. Robinson MD, McCarthy DJ, Smyth GK. edgeR: a Bioconductor package for differential expression analysis of digital gene expression data. *Bioinformatics* 2010;26:139-40.
7. Ayers M, Lunceford J, Nebozhyn M, *et al.* IFN-gamma-related mRNA profile predicts clinical response to PD-1 blockade. *J Clin Invest* 2017;127:2930-40.

8. Hanzelmann S, Castelo R, Guinney J. GSVA: gene set variation analysis for microarray and RNA-seq data. *BMC Bioinformatics* 2013;14:7.
9. Liberzon A, Subramanian A, Pinchback R, *et al.* Molecular signatures database (MSigDB) 3.0. *Bioinformatics* 2011;27:1739-40.
10. Stuart T, Butler A, Hoffman P, *et al.* Comprehensive Integration of Single-Cell Data. *Cell* 2019;177:1888-902 e21.
11. Germain PL, Sonrel A, Robinson MD. pipeComp, a general framework for the evaluation of computational pipelines, reveals performant single cell RNA-seq preprocessing tools. *Genome Biol* 2020;21:227.

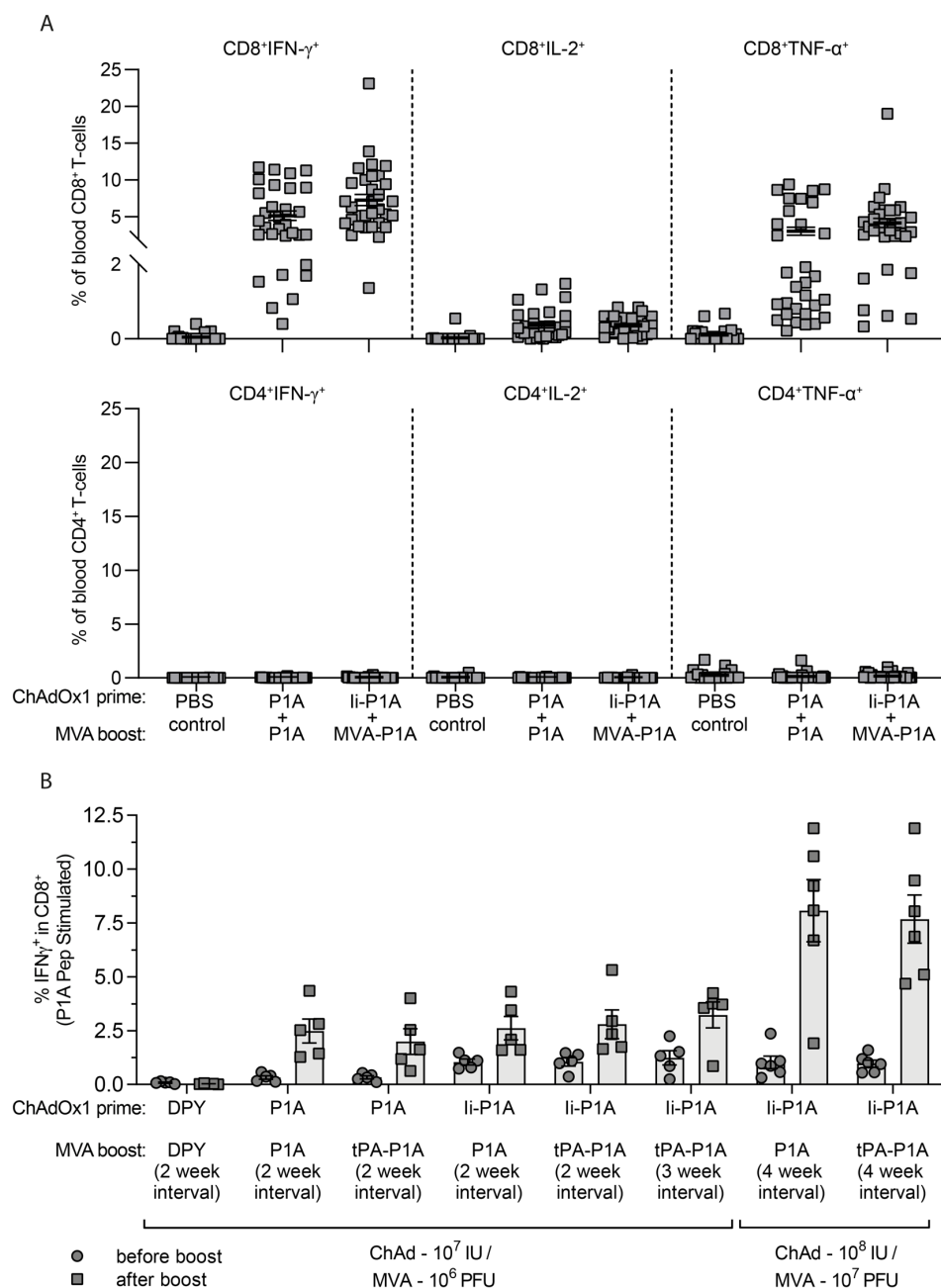


Figure S1: Blood P1A-specific T-cell responses induced by ChAdOx1/MVA P1A vaccination schemes. (A) DBA/2 mice received ChAdOx1-P1A (\pm li) and MVA-P1A vaccinations 4 weeks apart, and were bled after MVA vaccination as described in Fig. 1. PBMCs were stimulated *ex vivo* with 4 μ g/ml of P1A peptide pools, or a vehicle control (DMSO). The percentage of CD8⁺ and CD4⁺ T cells in the blood after prime-boost vaccination producing IFN- γ , IL-2 and TNF- α was then determined by ICS and flow cytometry. (B) DBA/2 mice were vaccinated with different vaccination regimes (as indicated) and bled 3 days before and 14 days after the MVA vaccination. PBMCs were stimulated *ex vivo* with 4 μ g/ml of P1A peptide pools, or a vehicle control (DMSO). The percentage of IFN- γ ⁺ CD8⁺ T cells after prime (closed circles) and boost (closed squares) in response to stimulation with P1A peptides vaccination was then determined by ICS and flow cytometry. Data are shown as the mean \pm SEM and each symbol represents an individual mouse.

McAuliffe et al.

Supplementary material

8

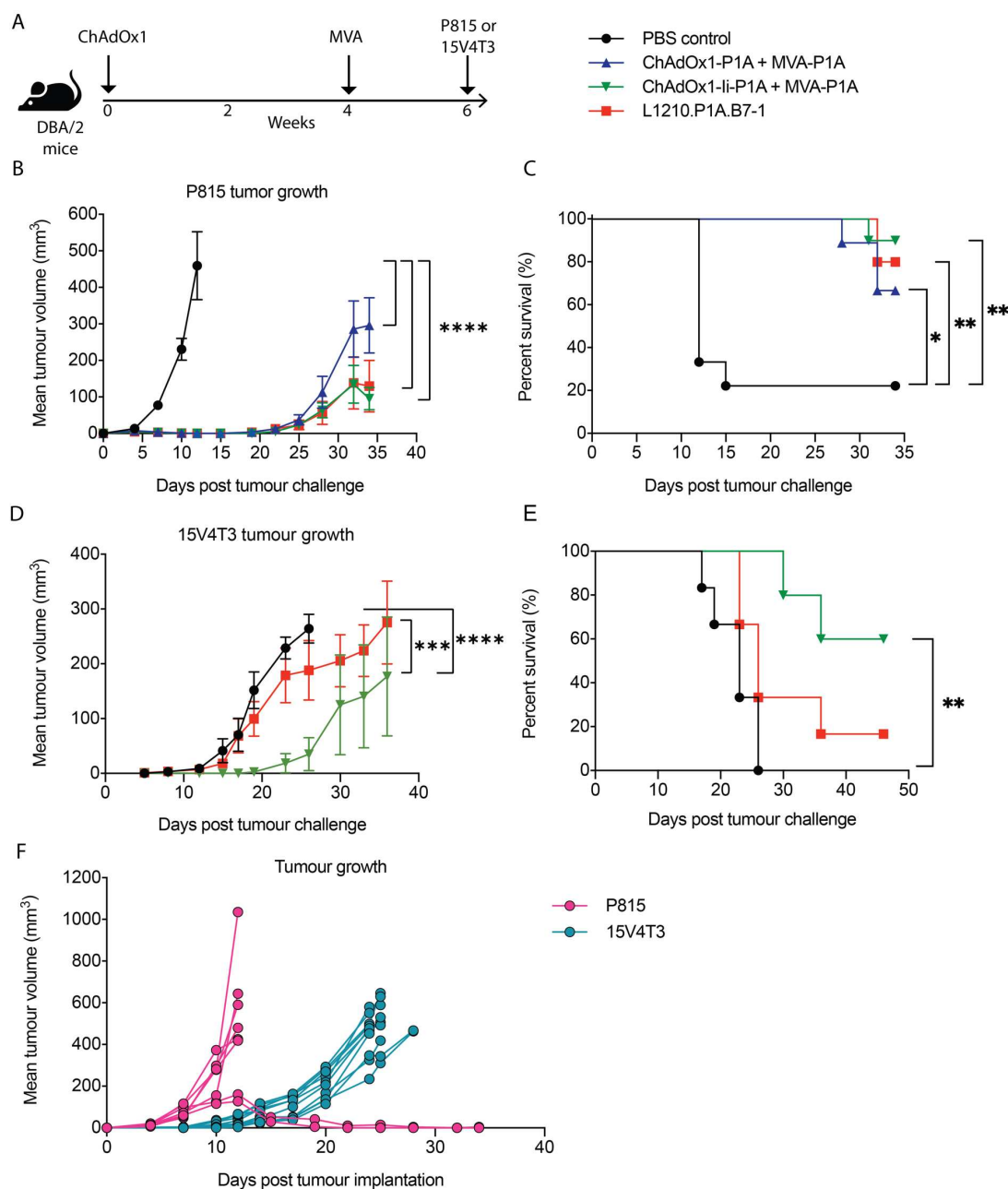


Figure S2: ChAdOx1/MVA P1A vaccination confers protection against P1A-expressing tumors. DBA/2 mice received a prime vaccination via intramuscular injection with 10^8 IU of ChAdOx1-P1A, ChAdOx1-li-P1A or a sham vaccination with PBS, then the ChAdOx1-P1A (\pm li) vaccinated mice received a boost vaccination with 10^7 PFU of MVA-P1A 4 weeks later. A fourth group received 1×10^6 L1210.P1A.B7-1 cells via intraperitoneal injection. Two weeks after the MVA boost vaccination, all mice were implanted with either 1.5×10^6 P815 or 1×10^6 15V4T3 cells in the right flank via subcutaneous (s.c.) injection. Tumor size was then measured and mice were sacrificed when tumor size reached 10 mm length in any direction. (A) Experimental timeline. (B-E) Mean tumor growth (B and D) and survival (C and E) for P815 and 15V4T3 challenged mice are shown. (F) Individual growth curves for P815 and 15V4T3 tumors from PBS control mice. Mean tumor growth data in B and D are presented as mean tumor volume (mm³) \pm SEM. Each group contained 5-10 mice, with data representative of 2 independent experiments. Statistically significant differences were determined by a two-way ANOVA followed by Tukey's post hoc test and statistical differences in survival data were determined by a log-rank test. *, $p \leq 0.05$, **, $p \leq 0.01$ ****, $p \leq 0.0001$.

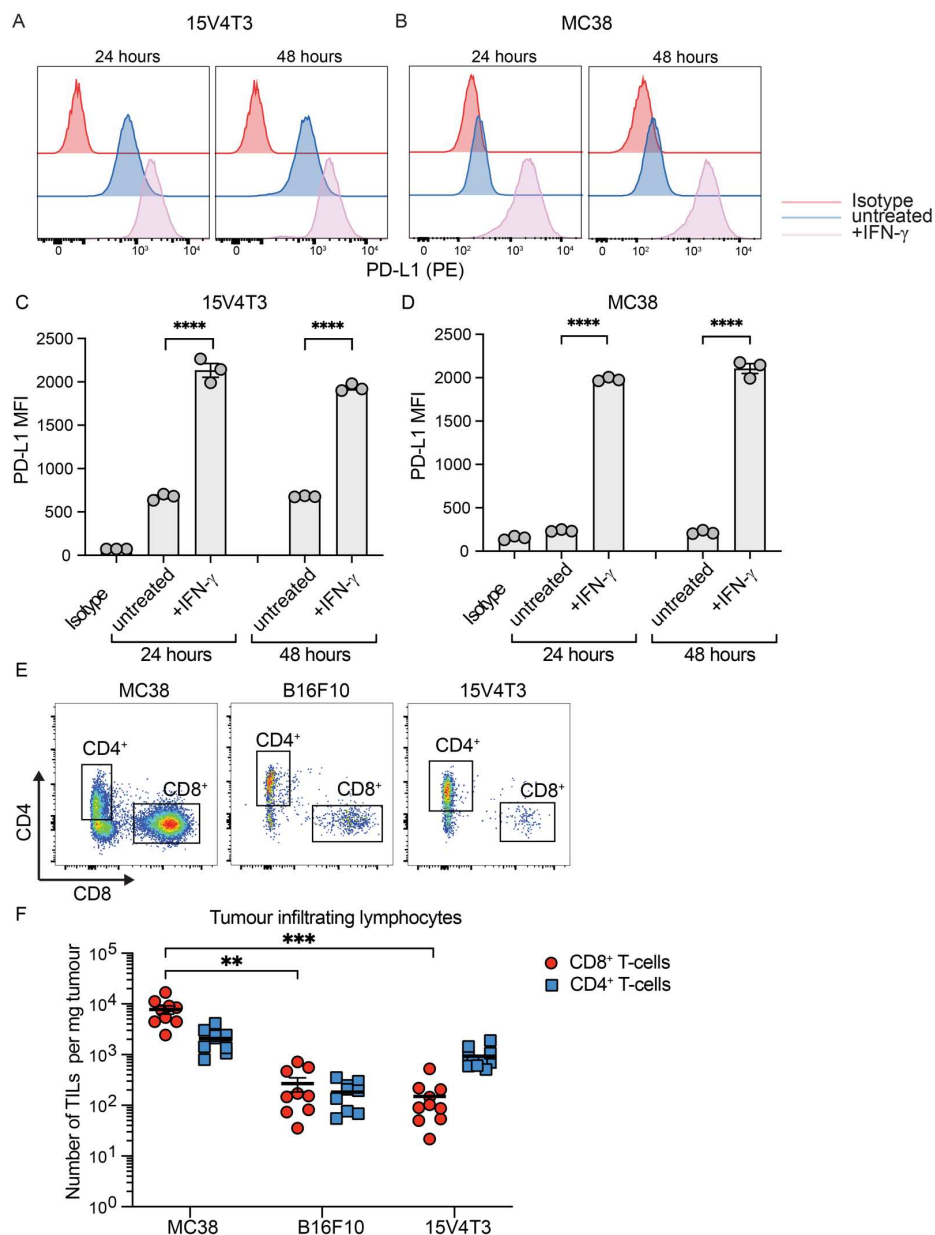


Figure S3: Surface PD-L1 expression level and CD8⁺ and CD4⁺ T-cell infiltration of murine tumor models.

15V4T3 and MC38 cells were cultured *in vitro* and stimulated with or without 20 ng/ml recombinant mouse IFN- γ for 24 or 48 hours. Cells were then stained with either PE-anti-PD-L1 or PE-IgG2b isotype control and the level of surface PD-L1 expression was assessed by flow cytometry. Representative flow cytometry histograms for PD-L1 expression level are shown for (A) 15V4T3 and (B) MC38. The PD-L1 mean fluorescence intensity (MFI) was calculated for (C) 15V4T3 and (D) MC38 cells. Each point shows an individual technical replicate ($n=3$ per group). Data are shown as mean \pm SEM. Statistical differences between each group were calculated by ordinary one-way ANOVA followed by Tukey's post hoc test. ****, $p \leq 0.0001$. (E, F) BL/6 mice were implanted with either 1×10^5 MC38 or B16F10 cells and DBA/2 mice with 1×10^6 15V4T3 cells via s.c. injection. Mice were sacrificed and tumors harvested when a size of 400-600 mm³ was reached. Tumors were dissociated and the immune infiltrate was analyzed by flow cytometry. (E) Representative flow cytometry plots of CD4⁺ and CD8⁺ T cells, gated on live CD3⁺ cells from MC38, B16F10 and 15V4T3 tumors. (F) Total numbers of tumor infiltrating CD4⁺ and CD8⁺ T cells. Data are shown as mean \pm SEM and each symbol represents an individual mouse, with $n=9/10$ mice per group. Statistically significant difference between groups was determined by a Kruskal-Wallis test with Dunn's multiple comparisons test. ** $p \leq 0.01$, ***, $p \leq 0.001$.

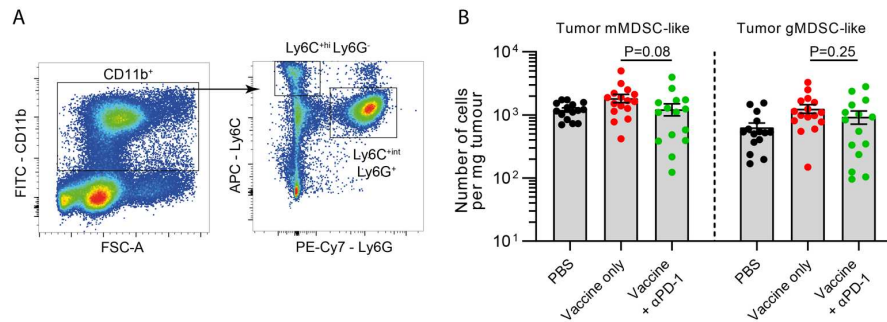


Figure S4: MDSC-like cell infiltration into 15V4T3 tumors. Mice bearing 15V4T3 tumors received ChAdOx/MVA P1A vaccination and were treated with anti-PD-1 as shown in Fig. 4A. Tumors were excised, processed to single cell suspension, and analyzed by flow cytometry. (A) Representative flow cytometry gating-strategy for mMDSC-like (CD11b⁺ Ly6C^{hi} Ly6G⁻) and gMDSC-like (CD11b⁺ Ly6C^{int} Ly6G⁺) cells. (B) Total numbers of tumor-infiltrating mMDSC-like and gMDSC-like cells as quantified by cytometry. Statistically significant differences between groups were compared by a Kruskal-Wallis test with Dunn's multiple comparisons test.

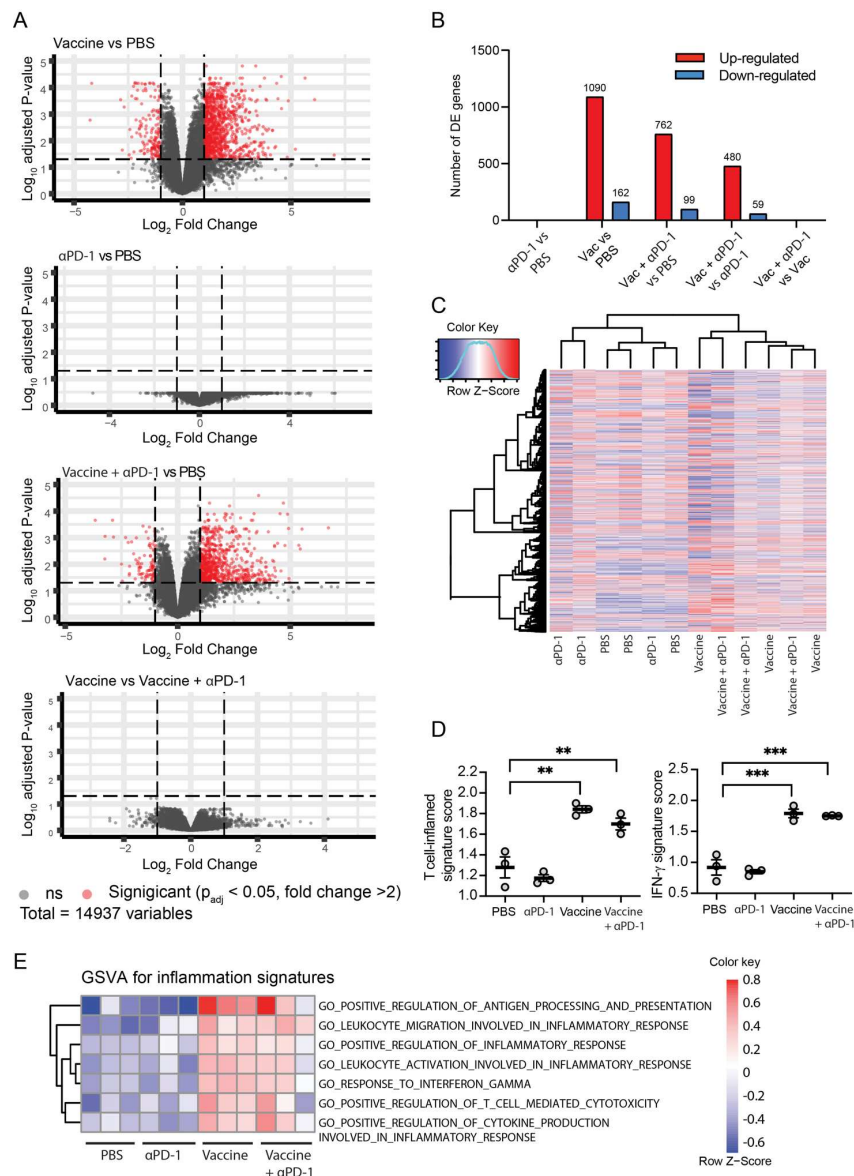


Figure S5: Bulk RNA-seq gene expression analysis of 15V4T3 tumors. 15V4T3 tumors were excised from the mice shown in Fig. 4 and RNA isolated from a small cutting of tumor tissue to analyze gene-expression at the transcriptional level. Tumor mRNA from each of 3 mice per group was sequenced on an Illumina NovaSeq 6000 as 150 bp paired-end reads. Following data processing, differential gene expression analysis between the anti-PD-1 only, vaccine only, and vaccine + anti-PD-1 combination treatment groups compared to the PBS control was performed using EdgeR software. (A) Volcano plots showing the distribution of differentially expressed genes (DEGs) between different experimental groups. Each point represents an individual gene, with significant DEGs shown in red. Dashed lines indicate the threshold set for significant differential expression of $\log_2FC > 1$ and $P_{adj} < 0.05$. (B) Number of DEGs identified in tumors in each of the experimental group comparisons (red upregulated, blue downregulated). (C) A heatmap showing log-CPM gene expression values of all expressed genes in the dataset for each sample. Expression across each gene (rows) has been scaled by calculation of a Z-score, indicated by the heatmap color key. Unsupervised hierarchical clustering was performed at both the gene (y-axis) and sample (x-axis) level and is shown in dendrogram format. (D) T cell-inflamed and IFN- γ gene expression signature scores for each sample. Data are shown as mean \pm SEM. Statistically significant differences between group gene signature scores were determined by an ordinary one-way ANOVA with Tukey's post hoc test. **, $p \leq 0.01$, ***, $p \leq 0.001$. (E) GSEA was performed for each of the indicated gene sets and the results are visualized on a heatmap.

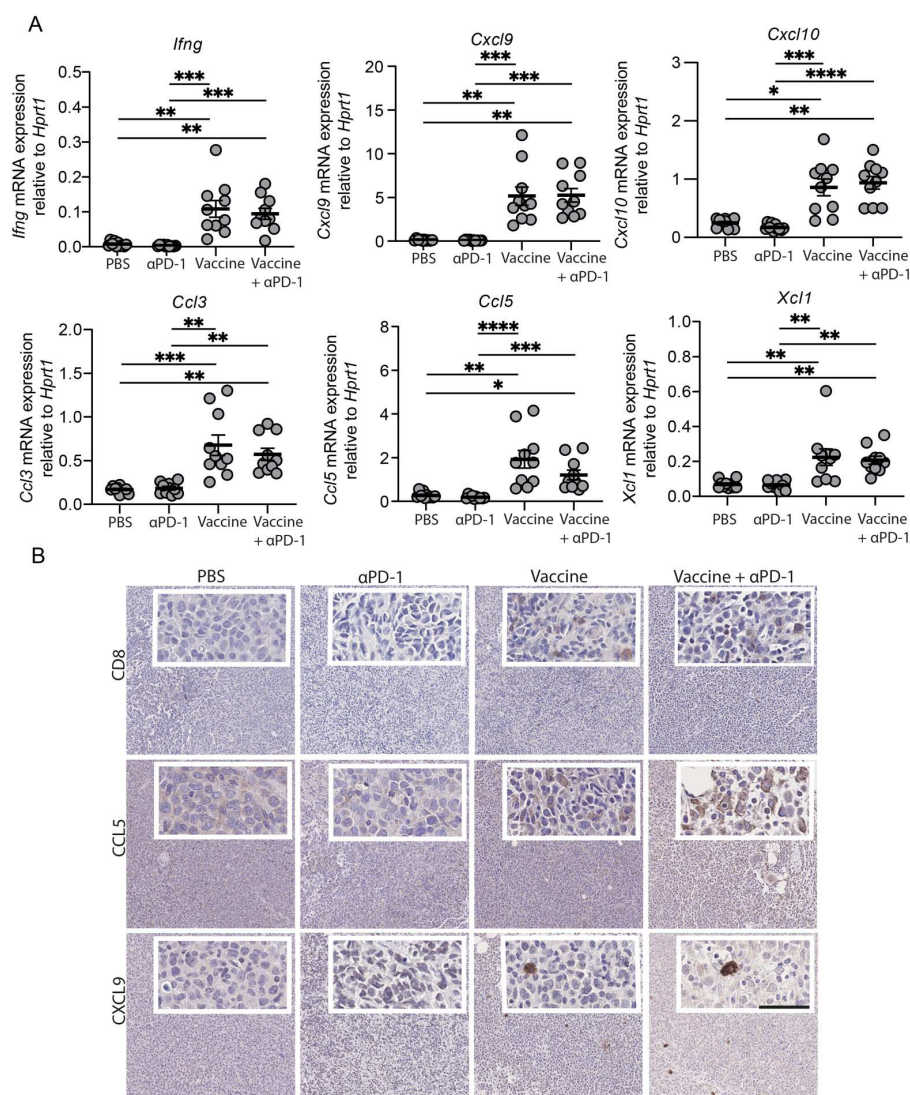


Figure S6: Assessment of pro-inflammatory mediator expression in the 15V4T3 tumor microenvironment.

15V4T3 tumors were excised from tumor-bearing mice vaccinated with ChAdOx1/MVA P1A and treated with anti-PD-1 as detailed in Fig. 4. (A) Tumor RNA was isolated to analyze gene expression of pro-inflammatory mediators. Expression of *Ifng*, *Cxcl9*, *Cxcl10*, *Ccl3*, *Ccl5*, and *Xcl1* mRNA in the tumor was quantified by RT-qPCR. Target gene mRNA expression level was normalized relative to *Hprt1* and is shown as $2^{-\Delta\text{Ct}}$. Data are presented as mean \pm SEM and each symbol represents an individual mouse, with $n=10$ mice per group. Statistically significant differences between groups were determined by a one-way ANOVA followed by Tukey's post hoc test. *, $p \leq 0.05$, **, $p \leq 0.01$, ***, $p \leq 0.001$ ****, $p \leq 0.0001$. (B) A cross-section cutting of tumor tissue was formalin-fixed and paraffin embedded (FFPE). Tissue sections (4 μm) were prepared from FFPE samples and stained with antibodies against CD8, CCL5 and CXCL9. Representative images of staining are shown of tumors from PBS control mice and each of the indicated treatment groups. Scale bars: 50 μm (inset) and 250 μm (overview).

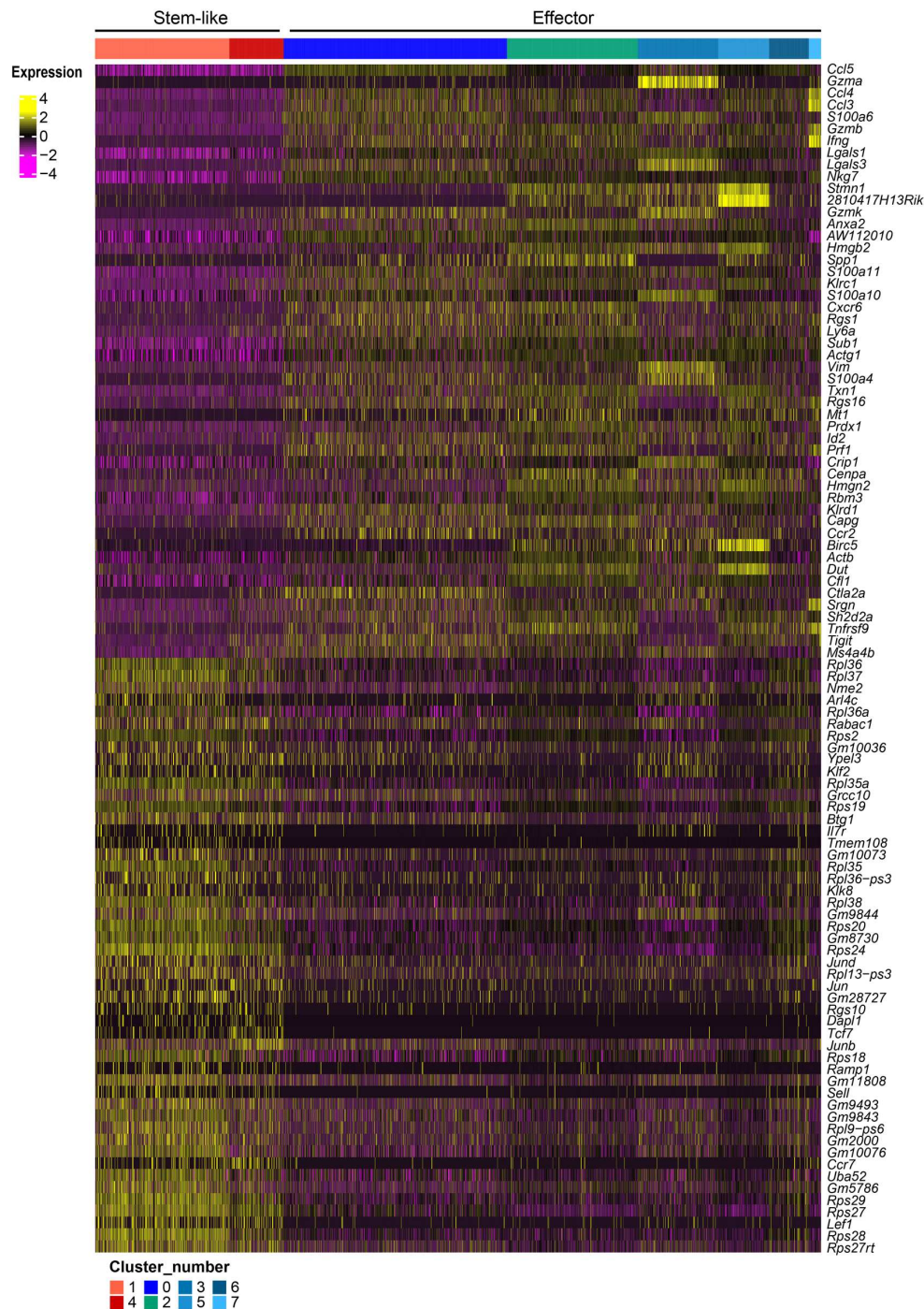


Figure S7: Heatmap of top 100 differentially expressed genes between stem-like and effector clusters identified by scRNA-seq of P1A₃₅₋₄₃-specific CD8⁺ T-cells. 15V4T3 tumor-bearing DBA/2 mice were vaccinated with ChAdOx1-ii-P1A/MVA P1A ± anti-PD-1 treatment (n=10 per group), tumors and spleens collected on day 25 and P1A₃₅₋₄₃-specific CD8⁺ T cells isolated via H-2L^d P1A₃₅₋₄₃ tetramer staining and FACS as described in Fig. 5A. The transcriptional profile of P1A₃₅₋₄₃-specific CD8⁺ T cells was determined via scRNA-seq using a 10X Genomics pipeline. Gene expression profiles of single cells separated into eight clusters by k-nearest neighbor clustering analysis using Seurat. The top 100 DEGs between the stem-like clusters and effector clusters are shown.

Table S2: P1A₃₅₋₄₃-specific CD8⁺ T-cell gene signatures identified by scRNA-seq

SpleenCombi_vs_ spleenVac_UP			SpleenVac_vs_ spleenCombi_UP		TumorCombi_vs_ tumorVac_UP	TumorVac_vs_ tumorCombi_UP
Jund	Uba52	Gm2000	Gzmk	Vim	Areg	Vps37b
Taf10	Set	Ets1	S100a6	Emp3	Gm10709	Ifi2712a
Chic2	Rps18	Nme1	Ccl4	Cdc42	H2-Q6	Rps8
Gnas	Arl2bp	Rps27rt	Ccl5	S100a4	Ccl4	Hsp90aa1
Alyref	Rpl9-ps6	Usf2	S100a10	Ywhaz	Gm8730	Cd7
Pcbp1	Emc10	Stk24	Klrc1	Arpc3	Gm9843	Slc3a2
Tprgl	Grb2	Rps2	Ms4a4b	Gimap7	Rps18	Rpl10
Ppp1cc	Rpl36-ps3	Gm10073	Nkg7	Actg1	Cox17	Pdcd1
Arf6	Hnrnpab	Gm5786	Ctla2a	Ifi2712a	Uba52	Hsp90ab1
Rac1	E2f4	Capns1	S100a11	Tmem50a	Ccl3	Hspd1
Btg1	Srsf2	Rpl36a	Ier3	Cf1	S100a4	Hnrnpa3
Pitpna	mt-Nd4	Ccni	Cd48	Thy1	Hcst	Serpib9
Dcun1d5	Glrx5	Rpl6l	Lgals1	Cyba	Rpl27-ps3	Serpib6b
Ypel3	Ptms	Gm28727	Lsp1	Lck	Rpl6l	Actb
Ube2s	Gm9493	Nme2	Sh2d1a	Hmgb2	Rps28	Hnrnpa1
Tmem243	Mkrn1	Rps26-ps1	Klrd1	Arpc1b	H2-Q1	Stat3
Tgfb1	Ccr7	2300009A05Rik	Ly6a	Cd3e		Mdh1
Hnrnp1	Ubald2	Gm8730	Calm2	AW112010		Eif4a1
Gnai2	Grk6	Rps20	Crip1	Actb		Sult2b1
Bag1	Mpnd	Gm9844	Lgals3	Tmsb4x		Stk17b
Cdc34	Aars	Rps19	Tigit	Cd52		Ifngr1
Ctbp1	Gnb1	Rpsa	Arl6ip5	Rac2		Gnb211
Klf2	H2-Ke6	Rpl35	Cd82	B2m		
Ybx1	Lamp1	Rpl12	Anxa2	Hcst		
Gm10076	Pdcd4	Gm11808	Laptm5	Pfn1		
Rab2a	1110008F13Rik	Rps21	Prr13	Sh3bgrl3		
March2	Rps28	Gm8186	Tagln2			
2310036O22Rik	Srm	Rps27	Sub1			
Mtch1	Gm10709	Rpl39	Ctsd			
Snf8	Lef1	Rps24	Sp100			
Bri3	Tmem108	Gm10260	Prdx1			
Arl4c	Rps29	Rpl3	S100a13			
Abhd17a	Erdr1	Rps7	Clic1			
Chmp4b	Efh2	Rpl38	Zyx			
H2afy	Rpl13-ps3	Rpl10a	Pycard			
Nsmce4a	Pcbd2		Gabarapl2			
Rap1b	Pnrc1		Myl6			

Table S3: Gene sets corresponding to CD8⁺ T-cell dysfunctional and progenitor gene signatures from other published studies

CD39- CD69-	MEL_EXHA UST_ Tirosh	CD8_G_Fel dman	Exhaust_1_Fe ldman	Exhaust_2_Fe ldman	Exhaust_3_Fe ldman	Mem_Eff_4_F eldman	Early.Act_5_F eldman	Mem_Eff_6_F eldman	LCMV_PROG.EX _Miller	B16_PROG.EX _Miller	Stem_like_Ba harom	TOX_Si G (Scott)	CD39+C D69+	CD8_G_Fel dman	LCMV_TERM.E X_Miller	B16_TERM.E X_Miller
KLF2	FCRL3	CD38	SPC25	GEM	CCL3	LMNA	ELL2	PLAC8	ID3	CCR6	Ctla4	IGKC	ENTPD1	IL7R	181001H11RIK	GZMD
AQP3	CD27	CCL3	CDC45	LAYN	EPSTI1	NR4A3	PFKFB3	S1PR1	CCR7	TCF7	Dapl1	AVIL	CD69	GPR183	ACOXL	GZMG
CLIC3	PRKCH	STMN1	ESCO2	VCAM1	CD38	GPR183	DTHD1	SORL1	CD83	AFF3	Socs3	TOX	RRM2	LMNA	CD244	GZMF
LINC008 61	B2M	MYO7A	CDC45	RDH10	FASLG	CDKN1A	SMAP2	SELL	BACE2	CXCR5	Tox	KLRB1C	TYMS	NR4A3	RASD2	GZME
CD8B	ITM2A	GOLIM4	ZWINT	FAM3C	IFI44L	CCR7	FKBP5	TCF7	ITGA7	DAPL1	Gpr183	MEGF1 1	CD8B	TCF7	FCER1G	DSC2
FAM65 B	TIGIT	VCAM1	SHCBP1	KIR2DL4	GIMAP6	S1PR1	AIM1	CCR7	TNFSF11	ID3	Nr4a2	SCD1	KIAA010 1	MGAT4A	OSGIN1	RASD2
FGFBP2	ID3	WARS	DLGAP5	TNFRSF18	TRAFD1	KDM6B	TMEM39A	IL7R	IL1R2	SLAMF6	Xcl1	RP23- 284K1. 6	CCL3	CD55	CCL6	CCL9
RASA3	GBP2	HAVCR2	RAD51	MTSS1	LGALS9	ELL2	NR4A3	MGAT4A	SOSTDC1	OTX1	Rgs16	PIF1	TUBA1B	AIM1	CD200R2	LTF
C10orf5 4	PDCD1	LGALS9	KIF18B	CADM1	CXCR6	TIPARP	PER1	FAM65B	DAPL1	CD22	Rpl12	TNFRSF 8	MKI67	PER1	GM10389	CCR1
SAMD3	KLRK1	ID3	RRM2	ENTPD1	RAB37	SC5D	TSPYL2	LTB	BMP7	TNFRSF25	Cd28	TMEM 163	UBE2C	FOSL2	CDK14	181001H11RIK
CD27	HSPA1A	PRDX3	BIRC5	ETV1	CCR5	PLK3	TTN	FLT3LG	GCAT	VAT1L	Id3	NR2F6	HLA- DOA2	EGR1	GPR56	IGSF5
FAIM3	SRGN	MCM5	TK1	AFAP1L2	ZBP1	CD55	TMEM2	PXN	FAM160A1	2610019F03RI K	Pou2f2	SERPIN B6B	CDK1	TSPYL2	AA467197	GZMC
S100A1 0	TNFRSF9	LSM2	HJURP	TNFRSF9	SAMD9L	NR4A1	IL6ST	A2M	IL7R	HECTD2	Junb	FGR	STMN1	YPEL5	CSF1	HTRA3
LYAR	TMBIM6	MTHFD1	UBE2C	NAB1	SIRPG	REL	NAB1	ATM	TNC	MAPK11	Eef1b2	LRRK1	IL5	CSRNP1	SLC16A10	LTB4R1
BIN1	TNFRSF1B	FASLG	CCNB2	PELI1	MX1	PBX4	IQGAP2	C20orf112	SERPINA9	ART3	Rplp0	SUV39 H2	NDFIP2	REL	GZMA	CD200R2
CTD- 3184A7. 4	CADM1	SNAP47	CENPW	DFNB31	HAVCR2	TNF	SLC7A5	GPR183	SLC43A1	TNFSF14	Rps15a	ESM1	DUSP6	SKIL	SFPI1	LGJ2
KANSL1 -AS1	ACTB	IFI35	GINS2	CTLA4	ACPS	IL7R	IPCEF1	EPB41	ART3	TNFSF8	Rps24	CENPE	CSF2	PIK3R1	RAC3	KLHL30
UBXN11	CD8A	SKA2	RAD51AP1	HSPB1	DDX60	RGCC	DCTN6	ADD3	PGCP	S1PR1	Ly6e	CCR2	XCL1	FOXP1	P2RY6	MGAT3
ZFP36L2	RGS2	NDUFB3	DTL	FKBP4	PDCD1	FOSL2	DUSP4	GRAP2	2610019F03RIK	FAM84A	Rpl6	KLRC1	UBE2S	RGCC	HTRA3	SERPINB9B
PPP2R5 C	FAIM3	FABP5	SPC24	NAMPTL	SH2D3C	SIK1	RANBP2	KLRG1	WNT3	PGCP	Tcf7	NTSDC 2	TOP2A	PFKFB3	IL20RA	GLIS1
LITAF	EID1	IFI27L2	CDC43	MYO7A	GPR174	CSRNP1	FAM177A1	GIMAP5	TUBA8	LIF	Zfp3611	CD244	HIST1H4 C	MYADM	E230016K23RIK	FCRL6
ZNF683	HSPB1	PTTG1	PKMYT1	CXCL13	RPS6KA1	GPR132	GABARAPL1	TC2N	CCR6	TREML2	Rpl10a	ASPM	AIF1	ZFP36L2	GPR97	PRPH
S1PR1	RNF19A	ENTPD1	MELK	GOLIM4	GBP5	GLUL	RGPD6	TXNIP	WNT1	SYNPO	Rps20	FAM20 A	TUBB	USP36	CHN2	LRRN4

McAuliffe et al.

Supplementary material

16

CD39-CD69-	MEL_EXHAUST_Tirosh	CD8_B_Fel dman	Exhaust_1_Fel dman	Exhaust_2_Fel dman	Exhaust_3_Fel dman	Mem_Eff_4_F eldman	Early_Act_5_F eldman	Mem_Eff_6_F eldman	LCMV_PROG.EX_Miller	B16_PROG.EX_Miller	Stem_like_Ba harom	TOX_Si G (Scott)	CD39+C D69+	CD8_G_Fel dman	LCMV_TERM.N.E X_Miller	B16_TERMIN.EX_Miller
TCF7	IFI16	EPST11	ANLN	PHLDA1	GBP1	KIAA1683	CTLA4	GIMAP2	SHANK1	SOSTDC1	Nsg2	ZDHHC2	CLSPN	TC2N	5031414D18RIK	HAVCR2
GIMAP4	LYST	PDCD1	CDC48	DNAJA4	PTPN6	RALGAPA1	CREM	TNFAIP8	OAF	WNT10A	Rpl36a	UBASH3B	IFI27	FAM177A1	VILL	CD244
MYC	PRF1	TRAFD1	KIAA0101	TGIF1	S100BPB	PRNP	ETS1	IL16	MAGED1	KCNMB1	Rps27a	SAPCD2	HMMR	BTG2	KLRA3	5830473C10RIK
S1PR4	STAT1	SIRPG	GGH	HAVCR2	IFI35	PRMT10	PNRC1		MORN4	CD40LG	Rgs1	SCD2	EGR1	TSC22D2	KLRA7	RASSF6
CD52	UBC	RGS3	AURKB	APLP2	OAS3	SORL1	ZFP36L2		SCMH1	DTX1	Actn1	KIF20B	KPNA2	FAM65B	RANBP17	GPR56
STK38	CD74	UBE2F	ASF1B	GPR56	SNAP47	FAM177A1	RGPD5		NSG2	DHRS3	Bcl2	CCR5	TPX2	STAT4	S1PR5	GZMB
NEAT1	IL2RG	SNRPD1	CDC20	BPGM	GIMAP4	CHMP1B	ZNF331		PAQR8	SELL	Tnfaip3	ACSL3	ZWINT	RGPD5	GM4956	1300014I06RIK
LGALS3	FYN	FIBP	NCAPG	SEC14L1	PARP9	ZC3H12A	CNOT6L		KIT	ST8SIA1	Cd69	WEE1	TK1	NEU1	TYROBP	FILIP1
GZMM	PTPN6	CLTA	DHFR	TNIP3	IFNG	TSC22D2	TGIF1		BC048355	TNFRSF13B	Rps9	HMMR	CD38	IFRD1	HEYL	CDKN2A
SORL1	HLA-DRB1	CXCL13	KIFC1	METRNL	SIT1	P2RY8	CXCL13		4930583H14RIK	CXCC5	Jun	SH2D5	UBE2T	PDE4B	TIFAB	GPR97
AL592183.1	HNRNPC	NMI	TYMS	HSPH1	PYCARD	NEU1	PDE4D		TWIST2	PLA2G4F	Rps8	MYO1E	NUSAP1	NR4A1	KLRA9	AA467197
R3HDM4	UBB	DNPH1	CKAP2L	KLRC2	RGS3	TCF7	RNF19A		SLC12A8	XCL1	Rpl29	CENPF	PCNA	AGPAT9	ADAM8	
MIAT	CD8B	PCNA	CLSPN	PMAIP1	XAF1	ZNF683			HSD3B7	CD83	Rps10	HAVCR2	CENPF	KLRB1C	CDH17	
ANXA4	HAVCR2	ACP5	MLF1IP	DUSP4	OAS2	MYADM			TCF7	CYR61	Fam46c	EOMES	H2AFX	ENTPD1	FCER1G	
LEF1	IRF8	MRPL28	TROAP	IGFLR1	C5orf56	ATP2B1			1700019D03RIK	KLF3	Rps28	PAK6	CRTAM	INSC	EPDR1	
TSC22D3	LAG3	FARSA	KIF2C	HSPA1A	GIMAP5	CREM			H2-OB	S1PR5	Rpl21	AHR	ASPM	RAB3IL1	CHL1	
IL7R	ATP5B	COX5A	WDR34	ZFAND2A	ABI3	OAT			ROPN1L	FAM160A1	Rpl7a	ARSB	GTSE1	CHIT1	IL1R2	
P2RY8	STAT3	MRPL51	CDK1	NDFIP2	SNX20	NFE2L2			XCL1	SH2B3	Sid1	KLRK1	TNFRSF18	GLP1R	CCL3	
PLEC	IGFLR1	SNRPE	KIF23	PAM	VAMP5	DNAJB9			CD22	TESPA1	Traf1	IL10	MYBL2	HDHD3	SPP1	
ERN1	MGEA5	RANBP1	PLK1	TP53INP1	IRF2	SKIL			FCRL1	LRIG1	Ppp1r15a	CKAP5	CKS1B	ATG9B	ACOXL	
TSPAN32	HSPA1B	NOP10	TOP2A	AH1	UBASH3A	DENND4A			TNP2	IL18	Crtam	ALYREF	SPC25	ARAP3	ENTPD1	
S100A4	COTL1	PYCARD	NUF2	UBE2F	PARP10	SERTAD1			MMP10	NSG2	Rps18	GEN1	CDKN3	TRPC1	CALCA	
SELL	VCAM1	GTF3C6	HMGB3	HSPA4	GIMAP7	YPEL5			FAM190A	SSPO	Rpl18a	IL24	IFNG	FAM19A3	CTNND2	
RASGRP2	HLA-DMA	CCR5	ASPM	ICOS	GBP4	BCL6			LTA	TBC1D4	Dusp1	ECT2	AURKA	SERPINB1A	NEB	
GADD45B	PDE7B	GSTO1	MCM2	CHORDC1	PVRIG	EGR1			DYNC2L1	SH3BP5	Uba52	MKI67	FEN1	QSER1	LY6G5B	

McAuliffe et al.

Supplementary material

17

CD39-CD69-	MEL_EXHAUST_Tirosh	CD8_B_Fel dman	Exhaust_1_Fel dman	Exhaust_2_Fel dman	Exhaust_3_Fel dman	Mem_Eff_4_F eldman	Early_Act_5_F eldman	Mem_Eff_6_F eldman	LCMV_PROG.EX_Miller	B16_PROG.EX_Miller	Stem_like_Ba harom	TOX_Si G (Scott)	CD39+C D69+	CD8_G_Fel dman	LCMV_TERM.N.E X_Miller	B16_TERMIN.EX_Miller
C11orf21	TBC1D4	OAS3	ORC6	TRPS1	CYTH4	PDE4B			DPYSL5	P2RX7	Rplp1	GTF2IR D1	GIN52		WDR31	UPP1
PIK3IP1	SNAP47	IGFLR1	CASC5	TBC1D4	DTX3L	ANXA1			AICDA	TNP2	Cd27	GZMA	CD40LG		RIPPLY3	AOAH
RNASET2	RGS4	HLA-DMA	CENPH	RALA	RHOC	SOD2			MNDA	SAMD3	Rpl15	HMGCS1	AURKB		PPP1R3B	MT2
S100A6	CLBL	STRA13	FEN1	CD82	SASH3	RNF125			TNFRSF26	FAM178B	Gnb2l1	BSPRY	NCAPG		STYK1	MREG
CCDC109B	TOX	HSD17B10	BRCA1	SEMA4A	CCL4L2	GADD45B			NME4	ZFP467	Cxcr3	ZBTB32	TNFSF10		CCL4	P2RY14
RAMP1	CALM2	VAMP5	MCM4	PON2	IFI6	SELK			DMRTA1	FAM81A	Rps4x	TUBB6	PLK1		FASL	ADORA3
RP11-640M9.1	ATHL1	NDUFAB1	TIMELESS	ACP5	BCAS4	RORA			STOM	SLC2A6	Rpl23a	BUB1	IL2RA		CDH17	EPAS1
GPR155	SPDYES	BATF	MKI67	CCDC64	IKZF3	SELL			TMOD2	GALNT14	Rpl27a	ANLN	AGPAT9		ATP8A2	PLXND1
TXNIP	DDX5	NDUF52	CDKN3	BHLHE40	GIMAP2	MXD1			SLFN5	GUCY1A3	Rpl34	SGOL2A	CCND2		ATF3	CDKN1A
CDC25B	SLA	C17orf49	APOBEC3B	NAMPT	ADORA2A	IFRD1			SLC22A17	PRSS2	Lag3	ULBP1	CENPE		4930515G01RIK	NPNT
ISG20	PTPRCAP	GN5	CCNB1	AHSA1	ARPC5L	PIK3R1			LIF	AQP3	Rplp2	LMNB1	CDC20		H2-DMB1	3300005D01RIK
TRADD	IRF9	PSMB2	TPX2	BANP	GYG1	TUBB4B			GM17384	GZMM	Rpl39	CCNA2	CCNB1		LRRN4	FGL2
CRBN	MATR3	PDIAG	NCAPG2	RHBDD2	SLFN5	HECA			PTER	F2RL1	Eef1a1	COBLL1	SMC2		GZMB	ASB2
GIMAP7	LITAF	COMMD3	KIF11	CREM	CHST12	MPZL3			GM4814	OAF	Rpl14	HRAS	BIRC5		SEPNI	PPP1R3B
C16orf54	TPI1	CD63	TCF19	SLC7A5	APOBEC3D	USP36			SLAMF6	COLQ	Rps3	STK39	TUBA1C		SEPT4	IL10
FBXL8	ETV1	PSMA4	UBE2T	CACYBP	WARS	INSIG1			CLDN10	CCR7	Rpl28	FANCB	CCNA2		KCNJ8	GPR35
ODF2L	PAM	SAE1	SPAG5	NUSAP1	UBE2L6	LTB			JAM3	TNFSF11	Naca	SRSF2	CKS2		MIRGPRE	ADRB1
LDLRAP1	ARID4B	ATP5J	BRCA2	STIP1	TMEM140	NR4A2			AFF3	TNFRSF26	PISD	MPP6	BIRC3		2900026A02RIK	MT1
MXI1	NAB1	MEA1	CCNA2	LRMP	CSK	SLC2A3			KIFC3	SLC15A1	Rpl17	FHL2	KRT7		PWWP2B	LAT2
RCBTB2	RAPGEF6	EXOSC9	BUB1B	PDE3B	F2R	PER1			CCDC116	BACH2	Rps19	KIF11	CENPW		ACTN2	D430041D05RIK
HSD17B11	LDHA	ARPC5L	CHEK1	RG52	CTSS	S100A10			TNS1	EMB	Inpp4b	NCAPG2	MCM7		ETV5	RG58
CLEC2B	WARS	BLOC1S1	BUB1	CCDC141	SLAMF7	AIM1			VIPR2	CXCR3	Zbtb32	FKBP5	ADAM19		CXCR6	OIT3
EMP3	RASSF5	HELLS	FANCI	SNAP47	CXCR3	MGAT4A			BCL2L14	NAPB	Rpl13	ANKLE1	TNF		TSGA10	RASL12
SH3BP5	OSBPL3	CXCR6	CENPM	DEDD2	CD27	CDC42EP3			GPR15	IL1RL1	Rps21	STIL	C15orf48		FGL2	SLC13A3
RP11-539L10.2	FAM3C	BCAS4	RNASEH2A	BTG3	PPP1R18	NDEL1			MAPK11	HEMGN	Limd2	PRC1	DLGAP5		PPP2R2C	SLC16A10

McAuliffe et al.

Supplementary material

18

CD39-CD69-	MEL_EXHAUST_Tirosh	CD8_B_Feldman	Exhaust_1_Feldman	Exhaust_2_Feldman	Exhaust_3_Feldman	Mem_Eff_4_Feldman	Early_Act_5_Feldman	Mem_Eff_6_Feldman	LCMV_PROG.EX_Miller	B16_PROG.EX_Miller	Stem_like_Baharom	TOX_SiG (Scott)	CD39+C D69+	CD8_G_Feldman	LCMV_TERM.N.E X_Miller	B16_TERMIN.EX_Miller
MIR142	TAP1	ETFB	HIRIP3	ITPRIP	TOX	IDI1			ENO2	ARC	Rpl37a	GPR141	DUSP5		EDARADD	PRF1
CLUAP1	HLA-DRB6	TXN2	MAD2L1	HSPA1B	CTSC	EIF4A3			9230110C19RIK	ANGPTL2	Rpl23	MTMR1	KIF11		FGD2	2810025M15RIK
YPEL3	FABP5	PTPN6	CCNF	GALNT2	SLAMF6	BIRC3			CXCR5	PRNP	Rps2	NFIL3	CCNB2		FCGR3	MYO10
SLCO3A1	CD200	SIT1	STMN1	TNFSF9	STAT1	TSPYL2			AFAP1	CD81	Rpl22	BUB1B	ACOT7		SYTL2	CD14
NOSIP	CTLA4	FKBP1A	SMC2	RANGAP1	FUT8	DCTN6			C3AR1	CRTAM	Rpsa	ITGAV	CASC5		IL10	CDKN2B
IL10RA	SNX9	COPZ1	CKS1B	PDCD1	IDH2	HSPH1			PRUNE2	POUGF1	Rpl8	SWAP70	PBK		6230409E13RIK	TSGA10
CD55	ETNK1	HLA-DRA	PAICS	DDX3Y	PCED1B	CDK17			SH3BP5	PLD4	Ighm	USP1	CDC43		HAVCR2	WNT10B
RP11-395B7.4	MALAT1	CDC123	NCAPH	ARIDS5B	BST2	DDX21			SFMBT2	DNASE1L3	Rpl11	ENTPD1	TESC		EPDR1	BCMO1
MED15	ZDHC6	AP2S1	ATAD5	DUSP10	PSMB10	PPP1R15B			NT5E	JUB	Cd9	RAC1	DUT		RAP5N	F2RL2
ATM	ARL6IP5	FUT8	PRC1	ZBTB1	STAT2	ZNF331			OASL2	ZHX2	Rps15	SGOL1	CENPM		SH3TC1	VIPR2
KLHL24	DUSP2	BST2	RFC5	SAMSN1	RNASET2	BTG2			1700025K23RIK	RAB37	Rpl32	NCAPG	KIF23		LRRC27	SYNPO2
ZNF276	HLA-DQB1	ATP6V1E1	CENPF	IRF4	RBCK1	AMD1			CCDC122	KLF4	Rpl24	PGP	ATAD2		PLEKHF1	2900026A02RIK
ANXA1	HNRNPK	CD2BP2	CENPN	CD2BP2	SEL1L3	SLC7A5			GSPT2	THA1	Fam101b	SPAG5	SGOL2		THRB	PPP2R2C
PLP2	DGKH	HLA-DQA1	CDCA7	SYNGR2	C14orf159	POLR3E			TREML2	SLC1A2	Rpl22l1	SLC25A13	TPM4		CISH	OPTN
AHNAK	LRMP	ZCRB1	CHTF18	CDK6	HLA-DRA	JMJD6			ISPD	GATSL3	Rps16	EMILIN2	AGTRAP		CCL3	DAB2IP
DDI2	H3F3B	MX1	CENPE	MCTP2	GZMA	CHD1			SELL	CMAH	Rpl5	TRIM59	MAD2L1		LAT2	ULBP1
VNN2	IDH2	TNFRSF9	WDR76	RAB27A	CD63	TAF13			AIP1	CAR2	Gimap6	CCNB1	NDC80		TMPRSS6	CCL4
VCL	TRAF5	SQRDL	FBXO5	HSPD1	DENND2D	VPS37B			CLEC12A	ARL4D	Ltb	MASTL	NUDT1		PRDM1	CLGN
EPB41	TBL1XR1	SERPINB1	CDCA7L	NFAT5	HLA-DQB1	GTF2B			KBTBD11	TRAT1	Pacsin1	ASB2	CDT1		CD7	CCR5
DND1	ANKRD10	PHPT1	RFC4	BATF	PRF1	PAF1			CXCL10	SESN3	Mif	SRSF9	CENPA		LYN	SV2C
MAPKA PK5-AS1	ALDOA	CALM3	POLD1	GZMB	CD84	BCAS2			LRRC49	BCL6	Rps23	CDC25C	RPL39L		XCR1	CD55
CDC425E1	LSP1	TOX	LRR1	NEU1	TIGIT	RGPD6			LRIG1	SLFN5	Smc4	MAN2A1	SHCBP1		GP49A	OSGIN1
PXN	PTPN7	SNRPC	RACGAP1	SYT11	CCL4L1	TUBA4A			P2RX7	MTMR7	Myc	KNTC1	CDCA8		F2RL2	CD200R4
SYNJ2	NSUN2	MRPS34	SNRNP25	CXCR6	PLSCR1	RASA3			SLC2A6	TLR1	Rpl3	AURKA	CEP55		CTNND2	CHN2
SIGIRR	RNF149	NUTF2	KNTC1	CNIH1	LAG3	GPCPD1			RAMP3	FAM53B	Cst7	TOPBP1	BRCA1		LIM2	SPATS2

McAuliffe et al.

Supplementary material

19

CD39-CD69-	MEL_EXHAUST_Tirosh	CD8_B_Feldman	Exhaust_1_Feldman	Exhaust_2_Feldman	Exhaust_3_Feldman	Mem_Eff_4_Feldman	Early_Act_5_Feldman	Mem_Eff_6_Feldman	LCMV_PROG.EX_Miller	B16_PROG.EX_Miller	Stem_like_Baharom	TOX_SIG (Scott)	CD39+C D69+	CD8_G_Feldman	LCMV_TERM.N.E X_Miller	B16_TERMIN.EX_Miller
PDE6G	CD2	NDUFS6	NUDT1	FCRL3	DAXX	RASGEF1B			ST6GAL1	CCDC64	Ifi2712a	CEP55	ORC6		CELA1	GIPC2
SLAMF6	SRSF1	PSMB3	ACOT7	CRTAM	PHF11	DNAJA1			ESPN		Rpl9	UGCG	CISH		ABI3	JAM2
TIMP1	GOLPH3	CHMP2A	CDK2	TTN	IGFLR1	FAM46C					Rpl37		MX1			
	HLA-A	SLC25A11	GMNN	TOX	ATP6V1E1	PTP4A1					Itpkb					
	LIMS1	SHFM1	TMEM106C	MORF4L2	HLA-DQA1	TUBA1A					Rps3a1					
	SDF4	TMEM179B	LIG1	TIGIT	CMTM3	KPNA2					Rpl35					
	ROCK1	EIF6	FANCG	DCTN6	DNAJC4	ZFAND5					Ccr7					
	EDEM1	ANXA5	MXD3	MTHFD2	LASP1	SLC38A2					Eef1g					
	APLP2	JAKMIP1	PCNA	FUT8	HLA-DMA	PLIN2					Rps27					
	ITK	TALDO1	C19orf48	GATA3	NCKAP1L	HEXIM1					Odc1					
	TRIM22	GLRX3	POLA2	STAT5B	OASL	TMEM123					Rpl35a					
	SPRY2	ANAPC11	POLE	AKIRIN2	TMEM179B	JUND					Slamf6					
	ACTG1	DUT	NDC80	WHSC1L1	CCL4	MTRNR2L1					Rps26					
	HLA-DPA1	PDCD5	MCM3	STAT3	USB1	GABARAPL1					Rps11					
	EWSR1	ATP5G3	CDK4	ZEB2	UBE2F	STAT4					Rpl4					
	SRSF4	CHMP5	SLC43A3	MSI2	CHMP5	ALG13					Gimap7					
	ESYT1	TWF2	TUBG1	B3GNT2	C19orf66	FOSB					Emb					
	LUC7L3	IDH2	NME1	EIF4E	PPM1M	GPR65					Rpl36					
	ARNT	MPG	HAUS8	CKS2	ST8SIA4	SDCBP					Rps7					
	GNAS	SNRPF	MCM7	HSPE1	YARS	HBP1					Kbtbd11					
	ARF6	NDUFC1	NCAPD2	KPNA2	TBC1D10C	MAP3K8					Fosb					
	ARPC5L	GBP1	RFC2	NGRN	DRAP1	RANBP2					Rps5					
	NCOA3	DCTN3	SHMT1	PTPN11	POLD4	FAM129A					Rps29					
	PAPOLA	ERH	DTYMK	SNAP23	TRAPP1	FOS					Rpl26					
	GFOD1	NDUFA12	PHF19	RASGEF1B	PKN1	DDIT3					lpcef1					

McAuliffe et al.

Supplementary material

20

CD39- CD69-	MEL_EXHA UST_ Tirosh	CD8_B_Fel dman	Exhaust_1_Fe ldman	Exhaust_2_Fe ldman	Exhaust_3_Fe ldman	Mem_Eff_4_F eldman	Early.Act_5_F eldman	Mem_Eff_6_F eldman	LCMV_PROG.EX _Miller	B16_PROG.EX _Miller	Stem_like_Ba harom	TOX_SI G (Scott)	CD39+C D69+	CD8_G_Fel dman	LCMV_TERM.NE X_Miller	B16_TERMIN.EX _Miller
	GPR174	LIMS1	POLD3	PFKFB3	JAKMIP1	CCNH					Rpl30					
	DDX3X	BANF1	DCTPP1	TNFRSF1B	LCP2	RGPD5					Rpl18					
	CAPRIN1	NDUFC2	POP7	CD27	CASP4	TUBA1C					Rps6					
	ARPC2	PSMC3	AHCY	TRIM13	APOL2	ATP1B3					Npm1					
	PDIA6	PON2	TEX30	ARNT	CASP1	GLIPR1					Psen2					
	SEMA4A	PRDX5	NUSAP1	SQSTM1	ABCA2	PRDM2										
	CSDE1	TMX1	DUT	MOB4	HLA-DRB5	EMD										
	PSMB9	STOML2	KIF18A	VPS37B	IFI27L2	HSPD1										
	NFATC1	RPS6KA1	MRPL17	ARL8B	SYNRG	MORF4L2										
	PAM	GGCT	TMEM140	ARHGAP30	IL21R											
	ATP5J2	CENPK	DNAJA1	IRF7	NFKBIA											
	GIMAP6	HAUS4	ZC3H7A	RARRES3	LYAR											
	NDUFB7	POLD2	GALM	HMOX2	DNAJB6											
	DBI	LMNB1	STAT5A	LSM2	TMBIM1											
	IFI6	BLM	CARD16	GZMH	PFKFB3											
	TSTA3	PRIM1	AMD1	ISG15	FAM65B											
	SSNA1	MT1E	RGCC	CHFR	MED29											
	ADORA2A	CDCA4	GOLGA4	TRPV2	B4GALT1											
	FDPS	RRM1	SDCBP	ZNHIT1	NXF1											
	CYC1	RBBP8	HNRNPLL	HLA-DPA1	BIRC2											
	PSMD4	NCAPD3	NR4A1	UBA7	ARHGAP26											
	FAM96A	TFDP1	BIRC3	ADAM8	SYAP1											
	OAS2	UNG	FBXW11	GOLIM4	DNTTIP2											
	ERCC1	ATAD2	TANK	SERPINB1	ETF1											
	PDHB	ACAT2	ASXL2	ATF6B	BTG1											

McAuliffe et al.

Supplementary material

21

CD39-CD69-	MEL_EXHAUST_Tirosh	CD8_G_Feldman	Exhaust_1_Feldman	Exhaust_2_Feldman	Exhaust_3_Feldman	Mem_Eff_4_Feldman	Early_Act_5_Feldman	Mem_Eff_6_Feldman	LCMV_PROG.EX_Miller	B16_PROG.EX_Miller	Stem_like_Baharom	TOX_SIG (Scott)	CD39+CD69+	CD8_G_Feldman	LCMV_TERM.NE X_Miller	B16_TERMIN.EX_Miller
		CD27	HADH	EIF5	SHISA5	PBXIP1										
		SNRPA	PAFAH1B3	FKBP1A	ITGB7	MKNK2										
		UBE2L3	YEATS4	GSPT1	TMBIM4	DEDD2										
		MDH1	RPA3	JMJD6	TRAF3IP3	AKIRIN1										
		SDHC	TIMM10	PRDM1	GPR171											
		PSMG2	MCM5	LAPTM4A	TRAF5											
		C11orf48	FANCD2	IL21R	ARHGEF3											
		PSMA2	RAD51C	ARPP19	PSMB8											
		C7orf73	ICMT	FABP5	IL2RB											
		MRPS16	HIST1H1D	SAR1B	APOBEC3G											
		MCM7	LSM5	LYST	CALCOCO2											
		SNX20	SSRP1	EZH2	MPHOSPH9											
		AK2	HIST1H4C	HERPUD1	DTHD1											
		RBBP7	DPYSL2	TRAF5	LY6E											
		TIGIT	TTF2	ANXA5	PPCS											
		TMPO	EEF1E1	ZNF331	CAPN1											
		CTSB	NUP37	UBE2B	GBP2											
		PARP1	EBNA1BP2	HBP1	PYHIN1											
		USB1	CCDC167	SYTL3	FKBP1A											
		MRPS7	MSH2	GTF3C1	NUDT22											
		NHP2	FH	FAS	CTSD											
		ATP5I	DDX11	SPPL2A	TRIM14											
		PSMC1	MRPL12	ATXN1	SLC25A45											
		VDAC1	PRDX4	GGA2	KLRD1											
		CARD16	DNAJC9	C5orf15	UCP2											

McAuliffe et al.

Supplementary material

22

CD3 9- CD6 9-	MEL_EXHA UST_ Tirosh	CD8_B_Fel dman	Exhaust_1_Fel dman	Exhaust_2_Fel dman	Exhaust_3_Fel dman	Mem_Eff_4_Fe ldman	Early.Act_5_Fe ldman	Mem_Eff_6_Fe ldman	LCMV_PROG.EX _Miller	B16_PROG.EX _Miller	Stem_like_Ba harom	TOX_ SIG (Scott)	CD39+CD 69+	CD8_G_Fel dman	LCMV_TERMN.EX _Miller	B16_TERMN.EX _Miller
		RNF181	ANAPC15	TSPYL2	UNC13D											
		PGAM1	ITGB3BP	PMF1	PSMB9											
		NT5C	MAGOHB	RBPJ	GSDMD											
		IRF2	MMS22L	POLR3E	IRF9											
		NUDT22	ACTL6A	RAPGEF1	MPG											
		NDUFA9	BOLA3	NOP58	MYO1F											
		SR1	USP1	EED	SLFN12L											
		GBP4	NABP2	CHST12	FERMT3											
		NDUFS8	MCM6	GTF2B	MUS81											
		PSMC2	RUVBL2	TMX4	APOL6											
		FBX5	VRK1	CCND2	C17orf62											
		PLSCR1	NCAPH2	PAPOLA	FCRL3											
		POLR2G	HELLS	FAM53B	ICAM3											
		COX8A	KIF22	CCT4	SP140											
		SLX1B	WHSC1	TRIM59												
		TRAPPC1	MYL6B	FXR1												
		ABI3	PDCD5	PPIL4												
		CBX5	SHMT2	LAG3												
		PSMD14	HIST1H1C	DNAJB6												
		UBE2L6	RANBP1	SMAP2												
		IFNG	SCCPDH	RP11-345J4.5												
		DECR1	HAUS1	GPBP1												
		ITGB1BP1	MRPS23	SERTAD1												
		AKR1B1	UBR7	PAG1												
		PSMA5	POLR2H	TRIM26												
				TCP1												
				AZIN1												